www.elsevier.com/locate/jbiomech

A soft-contact and wrench based approach to study grasp planning and execution

Tarkeshwar Singh, Satyajit Ambike

PII: S0021-9290(15)00513-8
DOI: http://dx.doi.org/10.1016/j.jbiomech.2015.09.019
Reference: BM7327

To appear in: *Journal of Biomechanics*

Received date: 31 January 2015
Revised date: 8 September 2015
Accepted date: 24 September 2015

Cite this article as: Tarkeshwar Singh and Satyajit Ambike, A soft-contact and wrench based approach to study grasp planning and execution, *Journal of Biomechanics,* http://dx.doi.org/10.1016/j.jbiomech.2015.09.019

A soft-contact and wrench based approach to study grasp planning and execution.

Tarkeshwar Singh[1], Satyajit Ambike[1,2]

Department of Kinesiology, The Pennsylvania State University, University Park, PA-16802

Department of Health and Kinesiology, Purdue University, West Lafayette, IN-47907

Keywords: Precision Grasps; Prehension; Grasp Stability; Wrench; Soft Contacts

Word Count: 2,398**.**

Address for correspondence:

Tarkeshwar Singh

Department of Exercise Science

University of South Carolina

921 Assembly Street

Columbia, SC 29208

Tel: (803) 777-5267

E-mail: tarkeshwar.singh@gmail.com

Introduction

Wrench models are widely used in robotics to study grasping. A variant of these models, which represents human digits as hard contacts, has been adapted for studying human prehension (León et al., 2012; Wells and Greig, 2001). However, human digits are soft contacts that apply a

four-component *wrench* (three force components and a *free moment* normal to the contact surface) on objects (Mason and Salisbury, 1985). Soft-contact models for human prehension have been proposed (Li and Kao, 2001; Xydas and Kao, 1999) but to the best of our knowledge, there are no papers that provide a methodology to implement a wrench based, three-dimensional (3D), soft-contact model for studying spatial prehension.

One compelling motive for building a soft-contact model is that hard contacts cannot model certain grasp conditions. For example, with hard contacts, static restraint of an object with two opposing digits is impossible. Imagine grasping a golf ball with the thumb and the index finger with cone-shaped thimbles glued to the fingertips (Figure 1A). While the thimble can apply forces in arbitrary directions, it cannot apply a free moment (a feature specific to soft contacts). This grasp cannot influence the rotation of the ball about the Z-axis. This is nontrivial because each thimble applies a three-dimensional wrench and the two thimbles together apply a six dimensional wrench that should be able to constrain the six kinematic degrees of freedom of the ball. However, the *grasp matrix* (defined below) for this two-digit contact is rank deficient (rank = 5), and hence the grasp is not *force-closure*[1] and therefore unstable.

Figure 1

Grasp matrices have been previously used to study grasp stability in robotic grasps (Howard and Kumar, 1996). In this paper, we obtain two indices (*grasp caliber* and *grasp intensity)* from the grasp matrix to quantify the effects of grasp planning (choice of digit placement on the object) and execution (choice of digit forces) on grasp stability in humans. We will show that

[1] Force-closure grasps are grasps in which the fingers can resist arbitrary external wrenches.

computing the grasp matrices in the appropriate coordinate frame is critical to studying grasp stability. The purpose of the current paper is to provide a step-by-step procedure for computing grasp matrices in different coordinate frames and to compute *grasp caliber* and *grasp intensity* to quantify grasp stability.

Methods

The wrench applied by the fingertips is related to the external wrench on the grasped object (**w**) by the *grasp matrix*, **G**:

$$-\mathbf{w} = [\mathbf{G}]\mathbf{f_C} \qquad (1)$$

The external wrench $\mathbf{w} \in R^p$ (p = 3 for planar and p = 6 for spatial analysis) is prescribed in the laboratory frame. $\mathbf{f_C} \in R^m$ ($m = m_1 + m_2 + \cdots + m_k$) is the concatenated *wrench intensity vector* applied by the digits and specified in local frames at the point of wrench application (see the next subsection). For digit k, m_k is the dimensionality of its wrench vector, and it depends on the type of contact model (3 for hard-contact and 4 for soft-contact models). The grasp matrix **[G]** $\in R^{p \times m}$ maps the fingertip wrenches to a laboratory-based reference frame. In the case of a three-digit tripod grasp with soft contacts (Figure 1B), $\mathbf{f_C}$ is a 12-dimensional vector ($[f_x, f_y, f_z, m_z] \times 3$ digits; f_x = force along the x axis, m_z = moment about the z axis, and so on), and **[G]** $\in R^{6 \times 12}$.

The concatenated *wrench intensity vector* (which we henceforth call '*wrench*') is written as:

$$\mathbf{f_C} = (\mathbf{f_{C_{TH}}}, \mathbf{f_{C_{IND}}}, \mathbf{f_{C_{MID}}}) \qquad (2)$$

where TH stands for thumb, IND for index and MID for middle finger.

Figure 2

Computing the Wrench for a Soft-Contact Model

We first obtain the wrench applied by a digit, $\mathbf{f}_{C_k}$ (k=TH, IND or MID), from the output of a 6D transducer. For a soft-contact model, $\mathbf{f}_{C_k}$ is (f_x, f_y, f_z, m_z), with the z-axis perpendicular to the sensor surface. Suppose that the instantaneous force reading is $\mathbf{p_k}$ =(p_x, p_y, p_z) in a reference frame at the center of the sensor and $\mathbf{q_k}$:=(q_x, q_y, q_z) is the moment about the same coordinate axes (Figure 2A). For a hard-contact model, **f**=**p, m**=**0** and there is a closed-form solution to the problem (Bicchi et al., 1993). For a soft-contact model, contact between the digit and the sensor surface occurs over a finite area but a unique *contact centroid* can be defined for a non-concave sensor surface. Then the contact problem for a soft-contact wrench can be defined as follows: For a given measurement ($\mathbf{p_k}$, $\mathbf{q_k}$), determine the location of the point of wrench application, $\mathbf{PWA_k}$, and the related wrench $\mathbf{f}_{C_k}$ =($\mathbf{f_k}$, $\mathbf{m_k}$) where $\mathbf{m_k}$=(0,0,m_z). For flat sensor surfaces, this reduces to computing the center-of-pressure on a force platform (Zatsiorsky, 2002).

Wrench Basis and Friction Cones

Grasp matrices are constructed using a *wrench basis,* $[\mathbf{B}_{C_k}] \in R^{p \times m_k}$ and a *friction cone,* FC (Murray et al., 1994). The dimension of the wrench basis depends on the contact model.

For a hard-contact model with friction,

$$\left[\mathbf{B}_{C_k}\right] = \begin{bmatrix} 1 & 0 & 0 \\ 0 & 1 & 0 \\ 0 & 0 & 1 \\ 0 & 0 & 0 \\ 0 & 0 & 0 \\ 0 & 0 & 0 \end{bmatrix} \qquad (3a)$$

For a soft-contact model,

$$\left[\mathbf{B}_{C_k}\right] = \begin{bmatrix} 1 & 0 & 0 & 0 \\ 0 & 1 & 0 & 0 \\ 0 & 0 & 1 & 0 \\ 0 & 0 & 0 & 0 \\ 0 & 0 & 0 & 0 \\ 0 & 0 & 0 & 1 \end{bmatrix} \qquad (3b)$$

The 6D contact wrench that is applied by a digit on the object is:

$$\mathbf{W}_{C_k} = \mathbf{B}_{C_k}\,\mathbf{f}_{C_k} \quad \text{where} \quad \mathbf{f}_{C_k} \in \mathrm{FC} \qquad (4)$$

That is, the set of wrenches that can be applied at a contact must lie within the friction-cone (FC) centered about the surface normal at the PWA. For a hard-contact model with friction,

$$\mathrm{FC} = \langle \mathbf{f} \in \mathrm{R}^3 : \sqrt{f_x^2 + f_y^2} \leq \mu_z f_z, f_z \geq 0 \rangle \qquad (5a)$$

f_z is the normal force, f_x and f_y are tangential forces, and μ_z (dimensionless) is the linear friction coefficient. For a soft-contact model with friction,

$$\mathrm{FC} = \langle \mathbf{f} \in \mathrm{R}^4 : \sqrt{f_x^2 + f_y^2} \leq \mu_z f_z, f_z \geq 0, |m_z| \leq \mu_{tor} f_z \rangle \qquad (5b)$$

where μ_{tor} (dimension of distance) is the torsional friction coefficient. We use the wrench basis in the next section to compute the grasp matrix.

Computing the Grasp Matrix

Once $\mathbf{f}_{\mathbf{C_k}}$ and $\mathbf{PWA_k}$ are obtained in the sensor frames, the grasp matrix in the appropriate reference frame is computed. The *adjoint matrix* transforms a soft-contact wrench ($\left[\mathbf{B}_{\mathrm{C_k}}\right]\mathbf{f}_{\mathbf{C_k}} \in R^6$) between two reference frames:

$$\mathbf{W}_{\mathrm{A}} = \mathbf{Ad}^{\mathrm{T}}_{(\mathrm{T}^{\mathrm{B}}_{\mathrm{A}})^{-1}}\mathbf{W}_{\mathrm{B}} \quad (6a)$$

where $\mathbf{W}_{\mathrm{B}}$ (the applied wrench in a frame B; we ignore the subscript k) is given by Equation 4 and

$$\mathbf{Ad}^{\mathrm{T}}_{(\mathrm{T}^{\mathrm{B}}_{\mathrm{A}})^{-1}} = \begin{bmatrix} \left[\mathrm{R}^{\mathrm{B}}_{\mathrm{A}}\right] & 0 \\ \widehat{\mathbf{p}}^{\mathrm{B}}_{\mathrm{A}}\left[\mathrm{R}^{\mathrm{B}}_{\mathrm{A}}\right] & \left[\mathrm{R}^{\mathrm{B}}_{\mathrm{A}}\right] \end{bmatrix} \in R^{6\times6} \quad (6b)$$

where $\left[\mathrm{R}^{\mathrm{B}}_{\mathrm{A}}\right] \in R^{3\times3}$ is a rotation matrix and $\mathrm{p}^{\mathrm{B}}_{\mathrm{A}} \in R^3$ is a position vector from the origin of frame A to the origin of frame B; and $\widehat{\mathbf{p}}^{\mathrm{B}}_{\mathrm{A}}$ is a 3×3 skew-symmetric matrix obtained from $\mathbf{p}^{\mathrm{B}}_{\mathrm{A}}$. Note that only kinematic data is required to determine the adjoint matrix. In Figure 1B, the object reference frame is placed at the object COM (OBJ). Then the wrench for an individual digit, k, is represented in the object frame as:

$$\mathbf{W}_{\mathrm{k_{COM}}} = \left[\mathbf{Ad}^{\mathrm{T}}_{\left(\mathbf{T}^{\mathbf{sensor_k}}_{\mathbf{COM}}\right)^{-1}}\right]\left[\mathbf{Ad}^{\mathrm{T}}_{\left(\mathrm{T}^{\mathbf{PWA_k}}_{\mathbf{sensor_k}}\right)^{-1}}\right]\left[\mathbf{B}_{\mathbf{C_k}}\right]\mathbf{f}_{\mathbf{C_k}}, \quad (7a)$$

and in the lab frame as:

$$\mathbf{W}_{\mathrm{k}_{\mathrm{Lab}}} = \left[\mathbf{Ad}^{\mathrm{T}}_{\left(\mathrm{T}^{\mathbf{COM}}_{\mathbf{Lab}}\right)^{-1}}\right]\left[\mathbf{Ad}^{\mathrm{T}}_{\left(\mathrm{T}^{\mathbf{sensor_k}}_{\mathbf{COM}}\right)^{-1}}\right]\left[\mathbf{Ad}^{\mathrm{T}}_{\left(\mathrm{T}^{\mathbf{PWA_k}}_{\mathbf{sensor_k}}\right)^{-1}}\right]\left[\mathbf{B}_{\mathbf{C_k}}\right]\mathbf{f}_{\mathbf{C_k}} \quad (7b)$$

where, for a digit 'k', sensor_k is the sensor coordinate frame and $\mathbf{PWA_k}$ is in the sensor_k reference frame. Therefore, the component of the grasp matrix for an individual digit in the object frame is given by:

$$\left[\mathbf{G}_{\mathrm{k}_{\mathrm{COM}}}\right] = \left[\mathbf{Ad}^{\mathrm{T}}_{\left(\mathrm{T}^{\mathbf{sensor_k}}_{\mathbf{COM}}\right)^{-1}}\right]\left[\mathbf{Ad}^{\mathrm{T}}_{\left(\mathrm{T}^{\mathbf{PWA_k}}_{\mathbf{sensor_k}}\right)^{-1}}\right]\left[\mathbf{B}_{\mathbf{C_k}}\right], \quad (8a)$$

and the component of the grasp matrix for a digit in the lab frame is:

$$\left[\mathbf{G}_{\mathrm{k}_{\mathrm{Lab}}}\right] = \left[\mathbf{Ad}^{\mathrm{T}}_{\left(\mathrm{T}^{\mathrm{COM}}_{\mathrm{Lab}}\right)^{-1}}\right]\left[\mathbf{Ad}^{\mathrm{T}}_{\left(\mathrm{T}^{\mathbf{sensor_k}}_{\mathbf{COM}}\right)^{-1}}\right]\left[\mathbf{Ad}^{\mathrm{T}}_{\left(\mathrm{T}^{\mathbf{PWA_k}}_{\mathbf{sensor_k}}\right)^{-1}}\right]\left[\mathbf{B}_{\mathbf{C_k}}\right] \quad (8b)$$

Then the grasp matrix for a three-digit tripod grasp shown in Figure 1B is

$$\mathbf{G_{Lab}} = \left[\mathbf{G}_{\mathrm{TH}_{\mathrm{Lab}}}\ \mathbf{G}_{\mathrm{IND}_{\mathrm{Lab}}}\ \mathbf{G}_{\mathrm{MID}_{\mathrm{Lab}}}\right] \quad (9)$$

For static equilibrium, the net digit wrench, $\mathbf{W}_{\mathrm{Lab}} \in R^6$, on the object balances the external wrench, **w**. Ignoring the 'Lab' subscript in the grasp matrix for simplicity,

$$-\mathbf{w} = \mathbf{W}_{\mathrm{Lab}} = \left[\mathbf{G}_{\mathrm{TH}}\ \mathbf{G}_{\mathrm{IND}}\ \mathbf{G}_{\mathrm{MID}}\right]\begin{bmatrix}\mathbf{f}_{\mathbf{C_{TH}}}\\ \mathbf{f}_{\mathbf{C_{IND}}}\\ \mathbf{f}_{\mathbf{C_{MID}}}\end{bmatrix} = [\mathbf{G}]\mathbf{f}_{\mathbf{C}} \quad (10)$$

Equation (10) is identical to Equation (1).

Grasp Caliber as a Measure of Grasp Planning

The choice of the appropriate coordinate frame is critical for investigating grasp stability. For example, the grasp matrices for the grasps in Figure 2B and Figure 2C are similar in the object reference frame but not in the laboratory reference frame. If the grasped container in Figure 2C contained a fluid, then a laboratory based coordinate frame is more appropriate to investigate stability since only this frame provides orientation information of the object.

Grasp matrices computed in the appropriate reference frames can be used to study grasp planning based on where participants place their digits on an object. For example, it is evident from visual inspection that the grasp in Figure 3A is more resistant to the shown perturbation than the grasps in Figures 3B and 3C. The three grasps are compared by computing the smallest singular value, s_n, of the respective grasp matrices (Li and Sastry, 1988). A zero singular value implies a rank deficient grasp matrix, (see next section) as well as grasp instability. Therefore, 's_n' measures the 'distance' of the grasp from instability, and we call 's_n' *grasp caliber*. Larger s_n values imply greater stability of the grasp to perturbations. s_n in Figure 3A is ~150 times that of the grasp in Figure 3B and √2 times the grasp in 3C.

Figure 3

Force-Closure, Internal Wrench and Grasp Intensity

Once the digits contact the object, subjects apply a wrench ($\mathbf{f_c}$) on the object. This wrench should satisfy the friction constraints and also resist perturbations. A grasp ([**G**], FC) is considered *force-closure* if it can resist an arbitrary external wrench without violating any friction constraints. The following are necessary conditions for force-closure:

a) [**G**] is surjective, i.e. rank(**G**)=6 in 3D.

b) **G** $(\mathbf{f_{C_H}})$=0 and $\mathbf{f_{C_H}}$ ∈ interior(FC). $\mathbf{f_{C_H}}$ is a *strictly internal wrench.*

where,

$$\mathbf{f_C} = \mathbf{f_{C_P}} + \mathbf{f_{C_H}} \quad (11)$$

and $\mathbf{f_{C_P}} \perp \mathbf{f_{C_H}}$ and $\mathbf{f_{C_H}}$ lies in the null space of [**G**]. $\mathbf{f_{C_P}}$ lies in the row space of [**G**] and is determined by computing the right inverse of [**G**], $[\mathbf{G_{R^+}}]=[\mathbf{G}]^{\mathrm{T}}([\mathbf{G}][\mathbf{G}]^{\mathrm{T}})^{-1}$ (Bicchi, 1994; Kerr and Roth, 1986). For condition a), the grasp matrix **G** is surjective in three dimensions as long as there are at least three non-collinear point contacts with friction or at least two soft contacts (Arimoto, 2008; Cole et al., 1989). The internal wrench $\mathbf{f_{C_H}}$ in condition b) does not affect the external wrench **w**, but plays an important role in maintaining a robust equilibrium of the object by squeezing it harder and thus countering external perturbations (Bicchi, 1995).

The terms of the RHS of Equation 11 can be written as

$$\mathbf{f_{C_P}} = -[\mathbf{G_{R^+}}]\mathbf{w}; \text{ (12a)}$$

$$\mathbf{f_{C_H}} = \mathrm{null}([\mathbf{G}])\boldsymbol{\lambda} \quad \text{(12b)}$$

λ is a vector and the norm, $||\boldsymbol{\lambda}||$, is a parameter that measures the *tightness* of the grip. We call $||\boldsymbol{\lambda}||$, *grasp intensity*. It is the second proposed index of grasp stability that quantifies the squeezing of the object above the safety margin (Burstedt et al., 1999), and therefore the ability to reject external disturbances.

To obtain || $\boldsymbol{\lambda}$ || from experimental data**,** we first obtain $\mathbf{f_C}$ (assuming that μ_z and μ_{tor} from Equation 5 are known)**.** $\mathbf{f_C}$ is constrained to be within the friction cone and is obtained from the sensor recordings (see section *Computing the Wrench for a Soft-Contact Model*). $\mathbf{f_{C_H}}$ can be obtained from Equations 11 and 12 and $\boldsymbol{\lambda}$ could then be obtained in the least square sense by computing the Moore-Penrose pseudoinverse of null([**G**]) or another optimization criteria (Buss et al., 1996; Pataky et al., 2004).

Experimental Application of *Grasp Caliber* and *Grasp Intensity*

One way to measure stability is to apply external perturbations using robots. Such robots have been used in reaching studies (Mussa-Ivaldi et al., 1985) but have not been used in grasping studies (though cf. Hadjiosif and Smith, 2015). Another method is to induce physiological perturbations like exercise-induced fatigue to study grasp stability. We performed a study where eight subjects (28.3±4.9 yrs) performed 60 trials (each trial 5 sec long) of a five digit precision grasp on a force handle (Figure 4A) that was instrumented with five six-component force/torque sensors (Nano17-R; ATI, Apex, NC, USA). Participants lifted the 8.96 N handle with their dominant hand and maintained it parallel to the horizontal. After these control trials, the participants performed a one-minute exercise to fatigue the thumb flexors (Figure 4B). Next, they repeated 60 grasping trials with a 20 s fatiguing exercise after every 5 trials to prevent recovery. They signed informed consent based on the procedures approved by the Office for Research Protection of The Pennsylvania State University, University Park, PA. Because of the small sample size, the Wilcoxon signed-rank test was performed to compare the before and during fatigue conditions. More details about the experiment are provided in (Singh et al., 2013).

Figure 4

Results and Discussion

The data showed significant effects of fatigue for all four components of the wrench (see Figure 5). In particular, the normal force (f_z) applied by the thumb, ring and little fingers decreased significantly during fatigue. The vertical tangential (f_x) forces, free moment (m_z) and the horizontal tangential force (f_y) applied by the thumb also changed significantly during fatigue.

Figure 5

Furthermore, during fatigue, participants reconfigured the PWAs and this resulted in significantly lower s_n values (see Figure 6A). This may be primarily due to the changes in the joint angles of the fingers during fatigue. Surprisingly, grasp intensity, $||\boldsymbol{\lambda}||$, was similar before and during fatigue (Figure 6B). This indicates that despite fatigue-induced changes in individual digit wrench components and *grasp caliber,* participants maintained *grasp intensity* to ensure a stable grasp. Perhaps, the heavy handle necessitated counteracting changes in the different wrench components (see Figure 5), resulting in only minor changes in *grasp intensity*.

Figure 6

The fact that choice of PWA (*grasp caliber)* is integrated with anticipatory force control (*grasp intensity)* based on the location of the center-of-mass of the object ('w' from Equation 1) has been shown within a planar framework (Lukos et al., 2007). This suggests that humans choose *grasp caliber* and *grasp intensity* based on 'w'. Our proposed method goes a step further and provides a method to experimentally manipulate 'w' and/or 'G' and quantify spatial grasp

planning and execution. We believe that then the two indices may provide a basis to independently quantify deficits in grasp planning and execution in certain clinical populations (e.g. schizophrenia (King et al., 2008) and autism (Stoit et al., 2013)). Furthermore, in experimental paradigms such as visuomotor rotation (Taylor et al., 2014), transcranial magnetic stimulation (Tunik et al., 2005), or experimentally induced loss of cutaneous sensation (Augurelle et al., 2003), *grasp caliber* and *grasp intensity* could be used as indices to study changes in grasp planning and execution.

Conclusions

In this paper we show how the tools from robotics can be employed to further our understanding of human prehension. We introduce two metrics, the *grasp caliber* and the *grasp intensity* to quantify how the choice of contact points and digit forces can provide insights into spatial grasp planning and execution.

Acknowledgements

The authors thank Drs. Vladimir M. Zatsiorsky and Mark Latash for inputs and for allowing us to reanalyze data (Figures 4-6) from a previously published study (Singh et al., 2013). The study was in part supported by NIH grants AG-018751, NS-035032, and AR-048563 to Drs. Zatsiorsky and Latash.

Conflict of Interest Statement

None declared.

References:

Arimoto, S., 2008. Control theory of multi-fingered hands: a modelling and analytical-mechanics approach for dexterity and intelligence. Springer, London. pp. 41-74.

Augurelle, A.-S., Smith, A.M., Lejeune, T., Thonnard, J.-L., 2003. Importance of cutaneous feedback in maintaining a secure grip during manipulation of hand-held objects. Journal of Neurophysiology 89, 665-671.

Bicchi, A., 1994. On the problem of decomposing grasp and manipulation forces in multiple whole-limb manipulation. Robotics and Autonomous Systems 13, 127-147.

Bicchi, A., 1995. On the closure properties of robotic grasping. The International Journal of Robotics Research 14, 319-334.

Bicchi, A., Salisbury, J.K., Brock, D.L., 1993. Contact sensing from force measurements. The International Journal of Robotics Research 12, 249-262.

Burstedt, M.K.O., Flanagan, J.R., Johansson, R.S., 1999. Control of grasp stability in humans under different frictional conditions during multidigit manipulation. Journal of Neurophysiology 82, 2393-2405.

Buss, M., Hashimoto, H., Moore, J.B., 1996. Dextrous hand grasping force optimization. Robotics and Automation, IEEE Transactions on 12, 406-418.

Cole, A.B.A., Hauser, J.E., Sastry, S.S., 1989. Kinematics and control of multifingered hands with rolling contact. IEEE Transactions on Automatic Control 34, 398-404.

Hadjiosif, A.M., Smith, M.A., 2015. Flexible control of safety margins for action based on environmental variability. Journal of Neuroscience 35, 9106-9121.

Howard, W.S., Kumar, V., 1996. On the stability of grasped objects. IEEE Transactions on Robotics and Automation 12, 904-917.

Kerr, J., Roth, B., 1986. Analysis of multifingered hands. The International Journal of Robotics Research 4, 3-17.

King, J.P., Christensen, B.K., Westwood, D.A., 2008. Grasping behavior in schizophrenia suggests selective impairment in the dorsal visual pathway. Journal of Abnormal Psychology 117, 799-811.

León, B., Sancho-Bru, J.L., Jarque-Bou, N.J., Morales, A., Roa, M.A., 2012. Evaluation of human prehension using grasp quality measures. International Journal of Advanced Robotic Systems 9, 1-12.

Li, Y., Kao, I., Year A review of modeling of soft-contact fingers and stiffness control for dextrous manipulation in robotics. In IEEE International Conference on Robotics and Automation.

Li, Z., Sastry, S.S., 1988. Task-oriented optimal grasping by multifingered robot hands. IEEE Journal of Robotics and Automation 4, 32-44.

Lukos, J., Ansuini, C., Santello, M., 2007. Choice of contact points during multidigit grasping: effect of predictability of object center of mass location. Journal of Neuroscience 27, 3894-3903.

Mason, M.T., Salisbury, J.K., 1985. Robot hands and the mechanics of manipulation. The MIT Press, Cambridge, MA.

Murray, R.M., Li, Z., Sastry, S.S., 1994. A mathematical introduction to robotic manipulation, First ed. CRC Press, Boca Raton, FL. pp. 217-222.

Mussa-Ivaldi, F.A., Hogan, N., Bizzi, E., 1985. Neural, mechanical, and geometric factors subserving arm posture in humans. Journal of Neuroscience 5, 2732-2743.

Pataky, T.C., Latash, M.L., Zatsiorsky, V.M., 2004. Prehension synergies during nonvertical grasping, II: Modeling and optimization. Biological Cybernetics 91, 231-242.

Singh, T., Zatsiorsky, V.M., Latash, M.L., 2013. Adaptations to fatigue of a single digit violate the principle of superposition in a multi-finger static prehension task. Experimental Brain Research 225, 589-602.

Stoit, A.M.B., van Schie, H.T., Slaats-Willemse, D.I.E., Buitelaar, J.K., 2013. Grasping motor impairments in autism: not action planning but movement execution is deficient. Journal of Autism and Developmental Disorders 43, 2793-2806.

Taylor, J.A., Krakauer, J.W., Ivry, R.B., 2014. Explicit and implicit contributions to learning in a sensorimotor adaptation task. Journal of Neuroscience 34, 3023-3032.

Tunik, E., Frey, S.H., Grafton, S.T., 2005. Virtual lesions of the anterior intraparietal area disrupt goal-dependent on-line adjustments of grasp. Nature Neuroscience 8, 505-511.

Wells, R., Greig, M., 2001. Characterizing human hand prehensile strength by force and moment wrench. Ergonomics 44, 1392-1402.

Xydas, N., Kao, I., 1999. Modeling of contact mechanics and friction limit surfaces for soft fingers in robotics, with experimental results. The International Journal of Robotics Research 18, 941-950.

Zatsiorsky, V.M., 2002. Kinetics of Human Motion, First ed. Human Kinetics, Champaign, IL. pp. 1-75.

Figure Captions

Figure 1: A) -The thimbles are glued to the glabrous skin of the digits, and they only allow forces to be exerted on the balls. The arrows show the direction and magnitude of the wrench vectors (f_{TH} and F_{IND}). If the golf ball is spun around the Z-axis, it would not be possible to resist the spin and bring the ball to a rotational equilibrium. B) - A schematic of a setup for a tripod grasp. Local frames are affixed to the center of the three force transducers (TH, IND and MID). A kinematic sensor provides spatial kinematic information of a reference frame attached to the object (OBJ) with respect to a fixed laboratory based reference frame (LAB).

Figure 2: A) -The sensor associated with a finger is shown. The local reference frame XYZ is affixed to the center of the sensor. The frame x'y'z' is at the point of wrench application (PWA). The fingertip applies a wrench (f_x, f_y, f_z, m_z) at the origin of x'y'z'. The wrench (f_x, f_y, f_z, m_z) is obtained from the recordings of the force sensor (p_x, p_y, p_z, q_x, q_y, q_z) using equations 3 and 4. B) and C) -The Grasp Matrix in the object reference frame is similar for the two grasps in B and C, but different in the laboratory reference frame. It is likely that the contents of the grasp in Figure 2c have spilled. Therefore, it is more meaningful to study stability in the laboratory reference frame instead of the object reference frame.

Figure 3: A) A two-digit grasp where the wrenches oppose each other. B) Another two-digit grasp where the wrenches don't oppose each other. C) The wrench components of the grasp are the same as the grasp shown in 3A but the digits are now placed on top of the cube. The red arrows show an arbitrary perturbation applied to the bottom of the cube. The magnitude of the g*rasp caliber* is largest for the grasp in Figure 3A, then Figure 3C, followed by Figure 3B.

Figure 4: A) A schematic representation of the force handle along with the attached force transducers, kinematic (Polhemus) sensor and the bull's eye leveler. B) The fatiguing setup for the right thumb.

Figure 5: A) Normal force, f_Z, before (blue) and during (green) fatigue for the thumb and four fingers. * indicates significant difference between the before and during fatigue conditions ($p < 0.05$). The results for vertical tangential force (f_X, panel B), horizontal tangential force (f_Y, panel C) and free moment (m_z, panel D) are also shown.

Figure 6: A) The smallest singular value (s_n) of the Grasp Matrix before (blue) and during fatigue (green) of the thumb. * indicates significant difference between the before and during fatigue conditions ($p < 0.05$). B) The *grasp intensity* ($||\lambda||$) for the two conditions. There were no differences between *grasp intensity* for the two conditions.

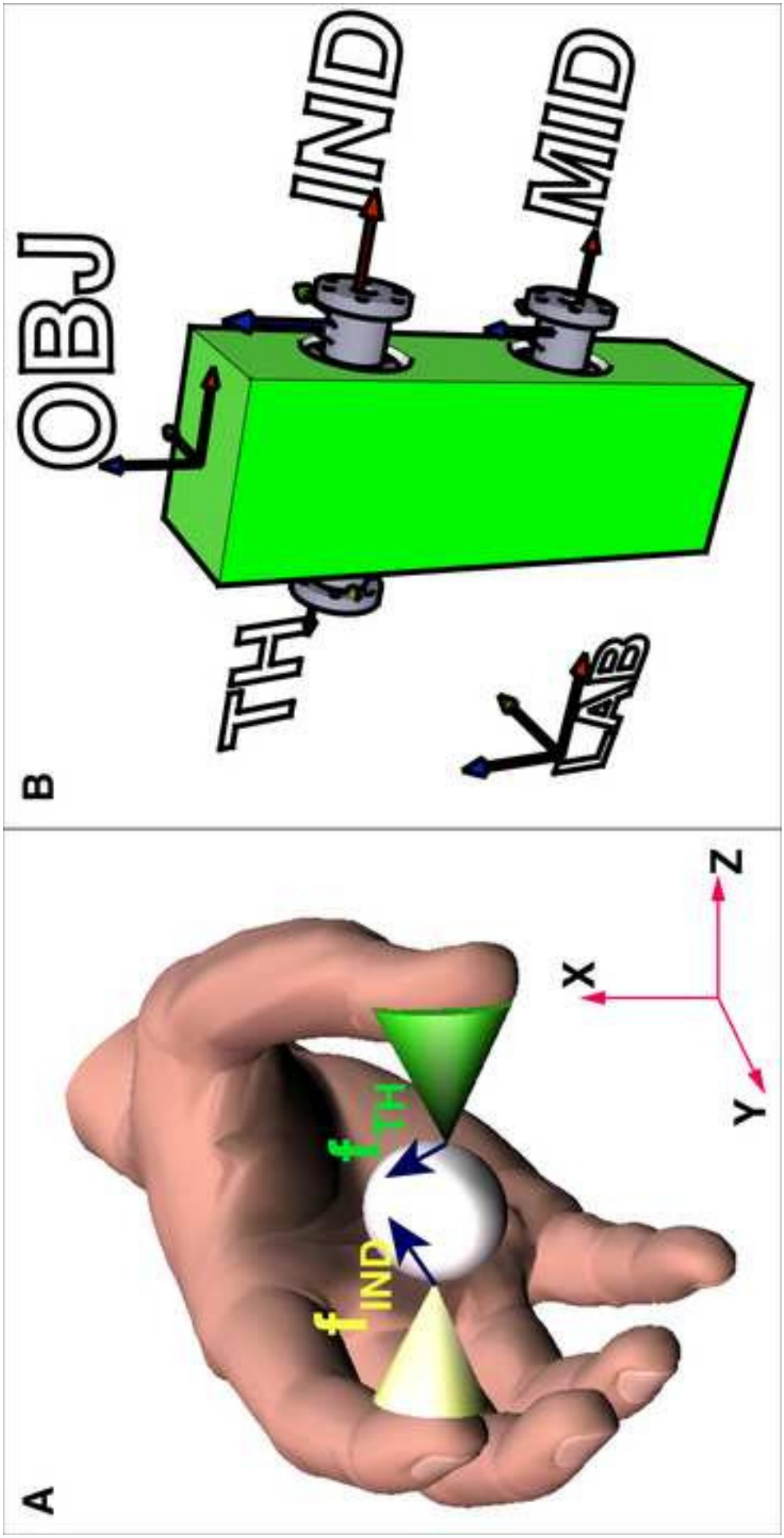

Figure 1

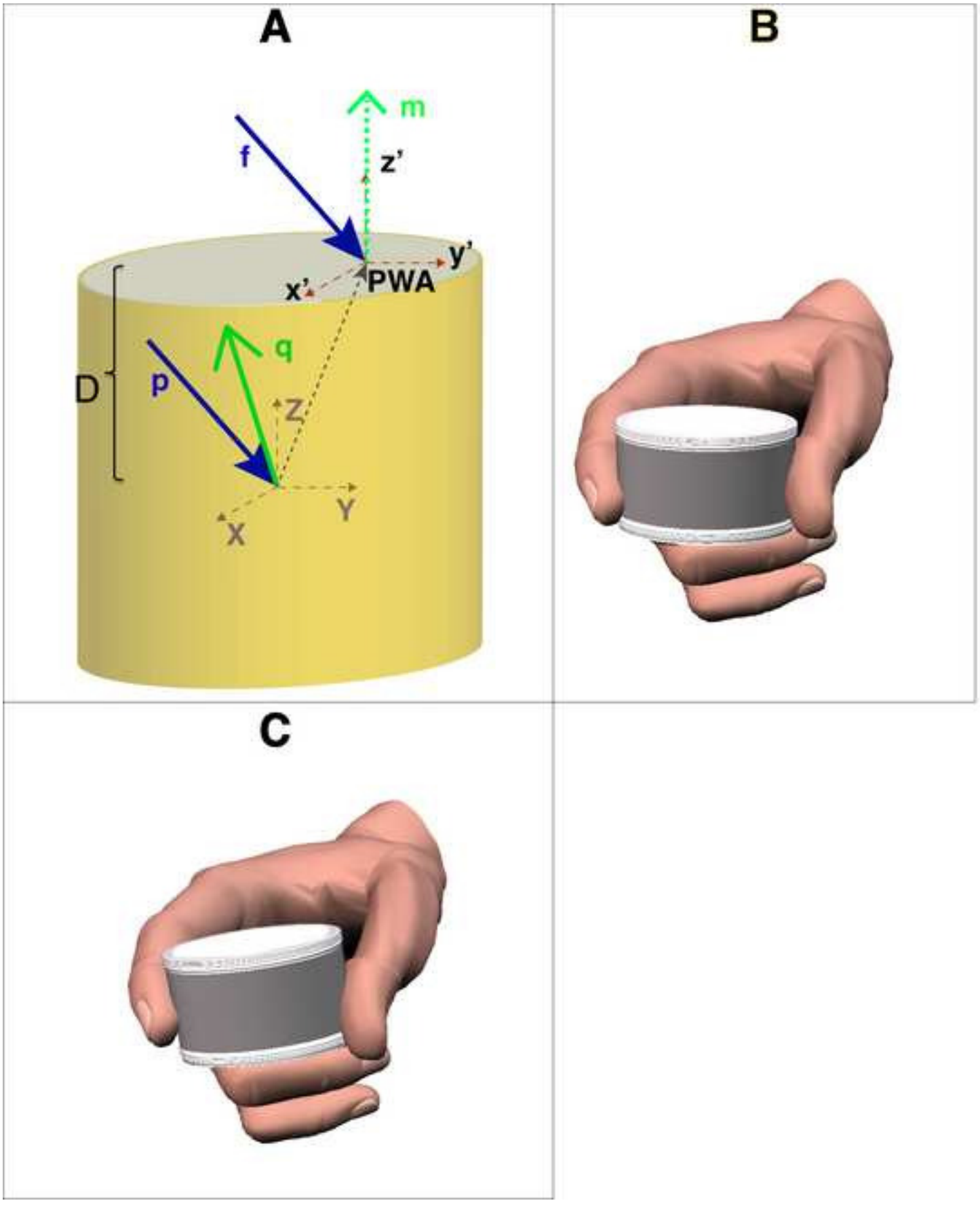

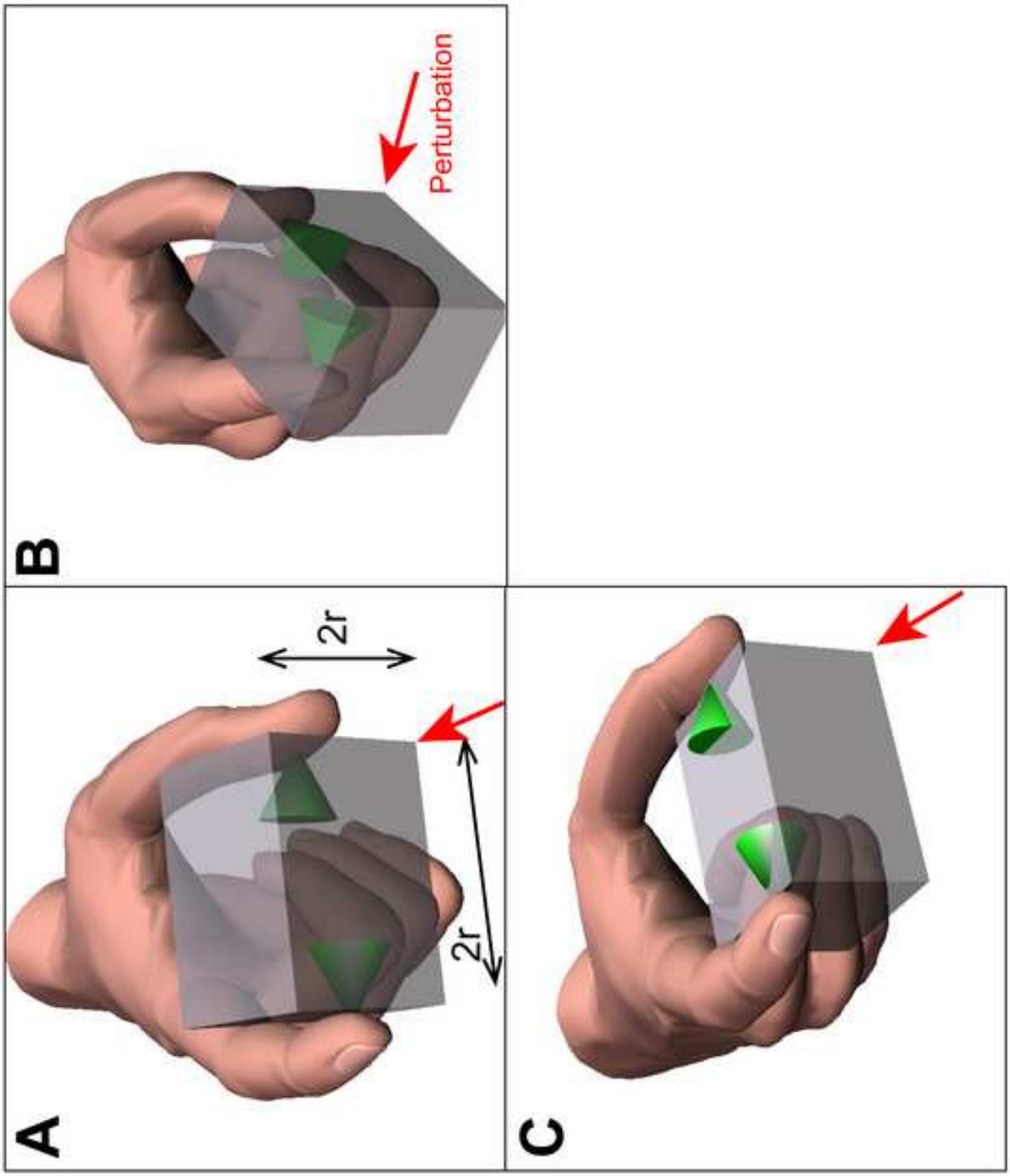

Figure 3

Figure 4

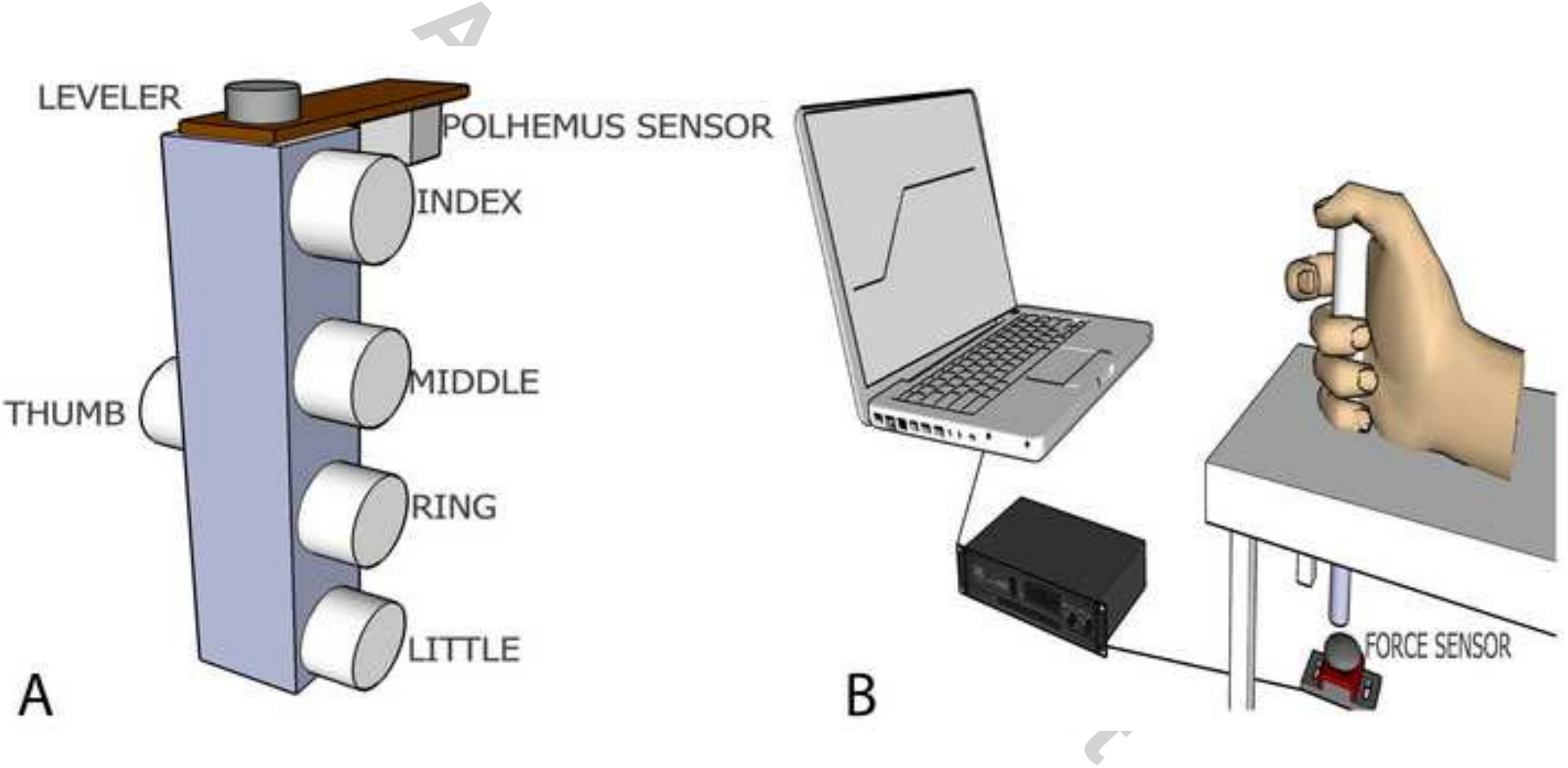

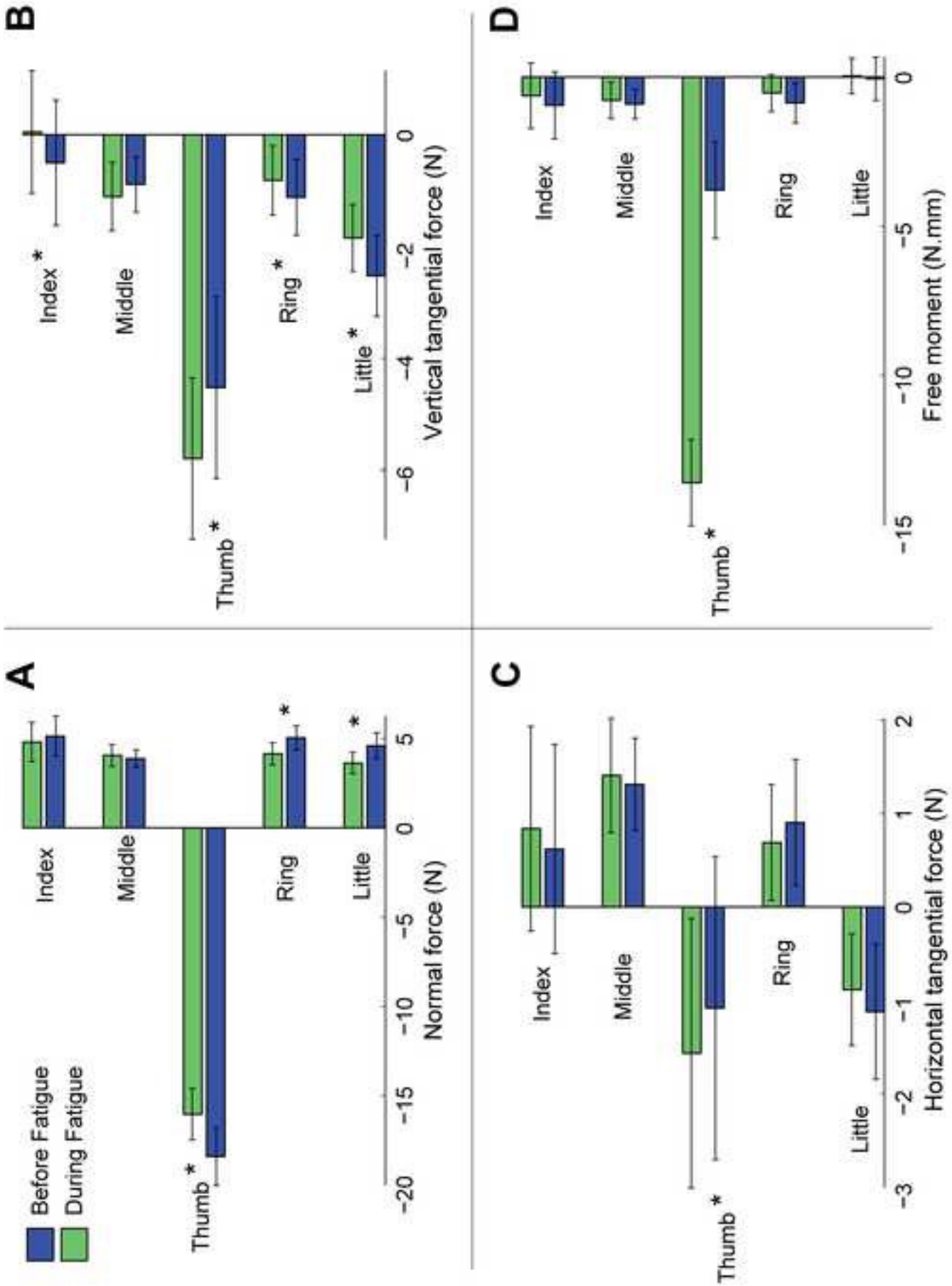

Figure 5

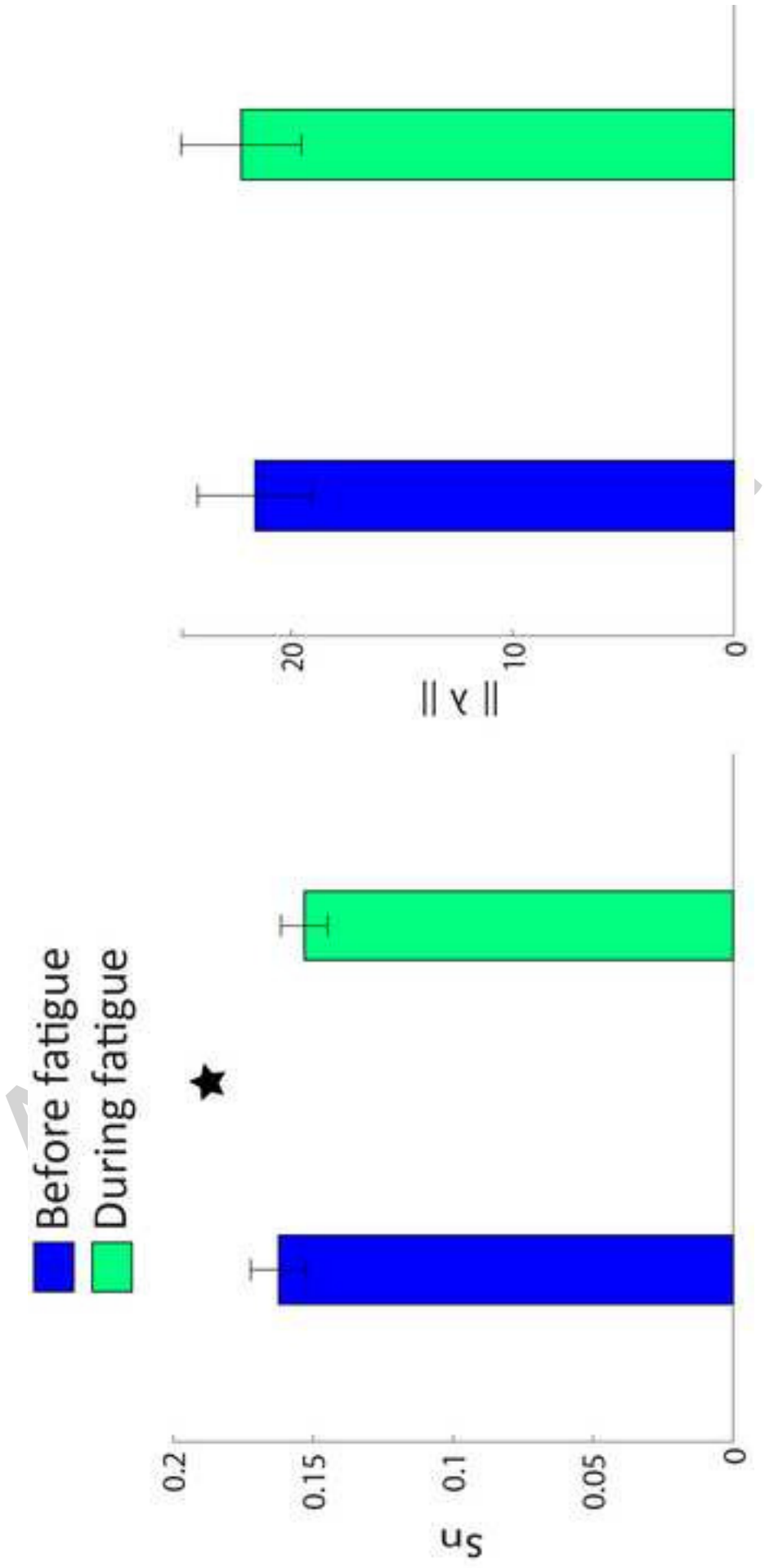
Before fatigue
During fatigue
s_n
0.2
0.15
0.1
0.05
0
$\|\lambda\|$
20
10
0

Figure 6